SLAC–PUB–12960
AARD–493
November/2007

Optical damage threshold of silicon for ultrafast infrared pulses*

Benjamin M. Cowan[a,b]

[a]Tech-X Corporation, 5621 Arapahoe Ave., Boulder, CO, USA 80303
[b]Stanford Linear Accelerator Center, 2575 Sand Hill Road, Menlo Park, CA, USA 94025

ABSTRACT

We present measurements of the optical damage threshold of crystalline silicon in air for ultrafast pulses in the near infrared. The wavelengths tested span a range from the telecommunications band at 1550 nm, extending to 2260 nm. We discuss the motivation for the measurements and give theoretical context. We then describe the experimental setup, diagnostics, and procedure. The results show a breakdown threshold of 0.2 J/cm^2 at 1550 nm and 1.06 ps FWHM pulse duration, and a weak dependence on wavelength.

Presented at Boulder Damage Symposium XXXIX, Boulder, CO, September 24–26, 2007.

Keywords: damage threshold, silicon, ultrafast, picosecond. infrared

1. INTRODUCTION

Silicon is an attractive material for high-power photonic components for several reasons. It is transparent in the near-infrared,[1] in particular in the telecommunications band at 1550 nm where many promising sources exist (see for instance Ref. 2). It has a high index of refraction at those wavelengths, which is generally required for the creation of photonic crystal structures with complete bandgaps.[3] Well-developed nanofabrication techniques exist for silicon due to its use in integrated circuits. In addition, its high resistance to ionizing radiation[4] makes it suitable for applications such as particle accelerator structures.[5] The sustainable fields in such structures are ultimately limited by optical damage to the material. Previously, the optical damage threshold has been measured for silicon at 800 nm.[6,7] Photonic structures relying on transparent materials would operate with silicon in the infrared. For accelerator applications in particular, sustainable gradient is a critical parameter, while the choice of operating wavelength remains open. Knowledge of damage thresholds for silicon at a range of wavelengths in the infrared would therefore serve to inform photonic structure design.

As discussed in Ref. 8, optical breakdown in dielectric materials occurs in four general steps: (1) Seed conduction electrons are generated by photoionization, (2) they are accelerated in the laser field and generate an avalanche by impact ionization, (3) the laser pulse heats the resulting plasma, and (4) the electron energy is transferred to the lattice, resulting in ablation. From the Keldysh theory of photoionization,[9] the limiting cases for the seed generation process are tunnel and multiphoton ionization. Should multiphoton ionization play a significant role, one would expect strong wavelength dependence of the damage threshold. The two regimes are differentiated by the parameter $\gamma = \omega\sqrt{m\Delta}/eE$, where ω is the angular frequency of the laser, m is the electron-hole reduced mass, Δ is the band gap, and E is the peak electric field of the laser. The condition $\gamma \ll 1$ indicates the tunneling regime, while $\gamma \gg 1$ indicates multiphoton ionization. In our case, with $\Delta = 1.1$ eV, $\lambda = 1550$ nm, and $E \sim 1$ GV/m, we can estimate $\gamma \sim 3$, so we are not operating clearly in one regime or the other. As a practical matter for photonic structure design, can we significantly increase the damage threshold by changing the wavelength? If multiphoton effects are important, operating at wavelengths beyond the two-photon threshold at 2214 nm might yield a significant increase in sustainable field.

*Work supported by Department of Energy contracts DE-AC02-76SF00515 (SLAC) and DE-FG03-97ER41043-II (LEAP).
Further author information: E-mail: benc@txcorp.com, Telephone: 1 303 996 7521

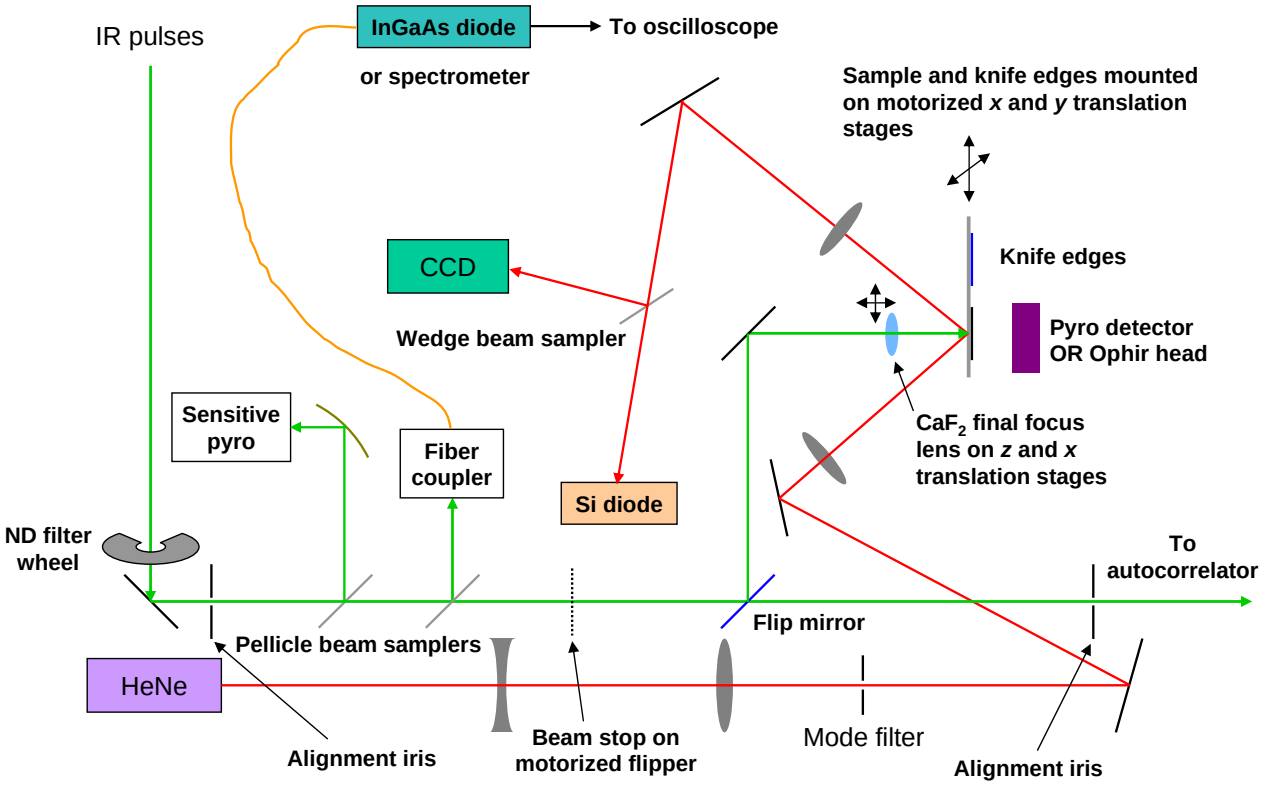

Figure 1. Schematic of the damage threshold measurement experiment.

2. EXPERIMENTAL SETUP AND PROCEDURE

As samples for the damage study, we used undoped crystalline silicon cut from a wafer with a (100) surface orientation. This was a pump-probe measurement in which a CW helium-neon laser was focused on the same spot on the sample as the infrared pulses and damage was detected by observing a decrease in reflected HeNe intensity. A schematic of the experiment is shown in Fig. 1. The experiment included the diagnostics necessary to measure both the pulse energy and the extent of the pulse in all three spatial dimensions, in order to obtain the energy density. We also measured the spectral content of the pulse to confirm that no residual light at shorter wavelengths was present.

The infrared pulses were generated by a commercial Spectra-Physics OPA-800 optical parametric amplifier (OPA) pumped by a Ti:sapphire laser system. The OPA produced pulses with energy $\geq 20\,\mu$J at a repetition rate of 240 Hz; the experiment detected multiple-shot damage. The pulse widths varied between 0.66 and 1.12 ps, depending on wavelength. The pulses first passed through a neutral density filter to control the intensity. They then passed through several diagnostic pellicle beam samplers. The first of these directed a small fraction of the pulse energy into a pyroelectric detector that served as the main pulse energy diagnostic. An off-axis parabolic mirror was used to focus the pulse just enough to ensure that all the energy was captured by the detector. The second beam pick-off directed a small amount of the pulse energy into a multimode fiber. This was connected to an InGaAs photodiode to optimally align the fiber, and then to an optical spectrum analyzer (OSA) to measure the spectrum.

After the diagnostic pick-offs the pulses were directed by a flip mirror toward the sample. They were normally incident on the sample, focused by a CaF_2 lens to minimize dispersion, while the HeNe beam was incident at an angle. The sample was mounted vertically on motorized translation stages with motion in the plane of the sample, and was oriented during initial setup so that it was parallel to the directions of motion of the stages. Razor blades were mounted in the same plane as the sample to conduct knife-edge transverse spot size measurements. A photograph of the setup is shown in Fig. 2.

With the flip mirror down, the pulses would proceed to an autocorrelator setup used for measuring the pulse duration. A schematic of the autocorrelator is shown in Fig. 3. The infrared pulses were split into two arms of an interferometer with

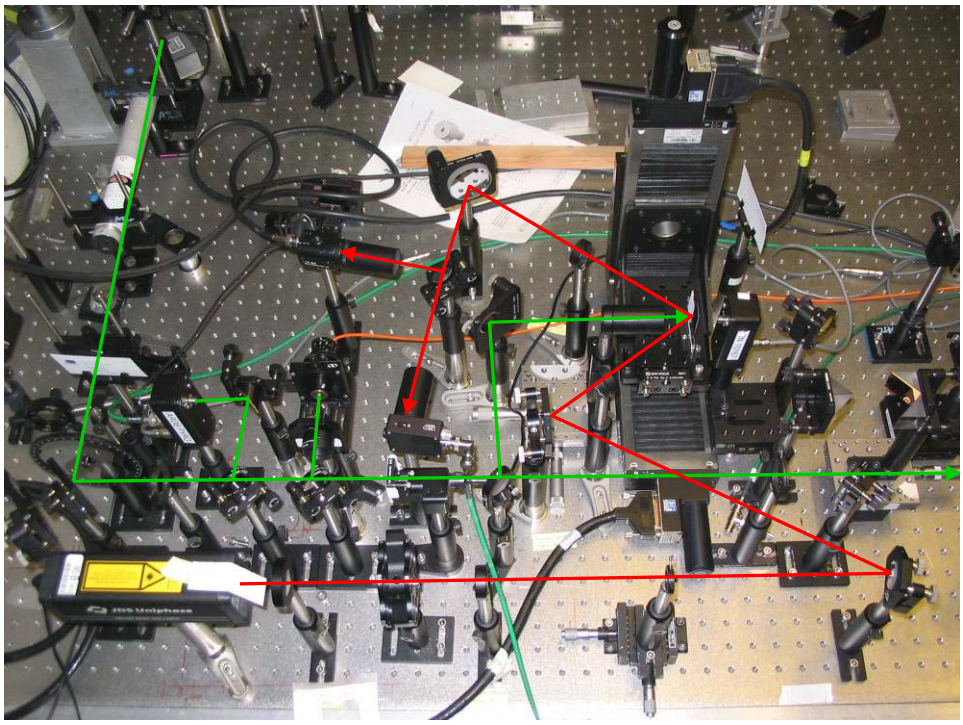

Figure 2. Photo of the damage threshold measurement experiment. The path of the infrared pulses is drawn in green, and the HeNe path in red.

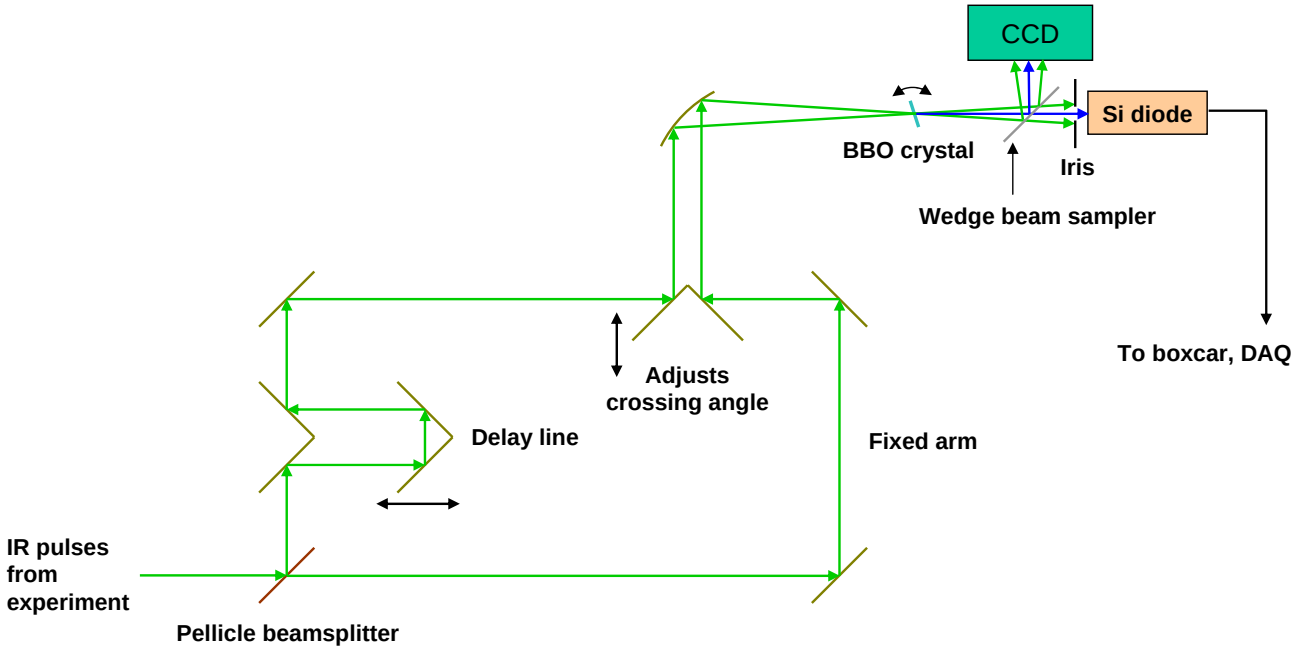

Figure 3. Schematic of the autocorrelator.

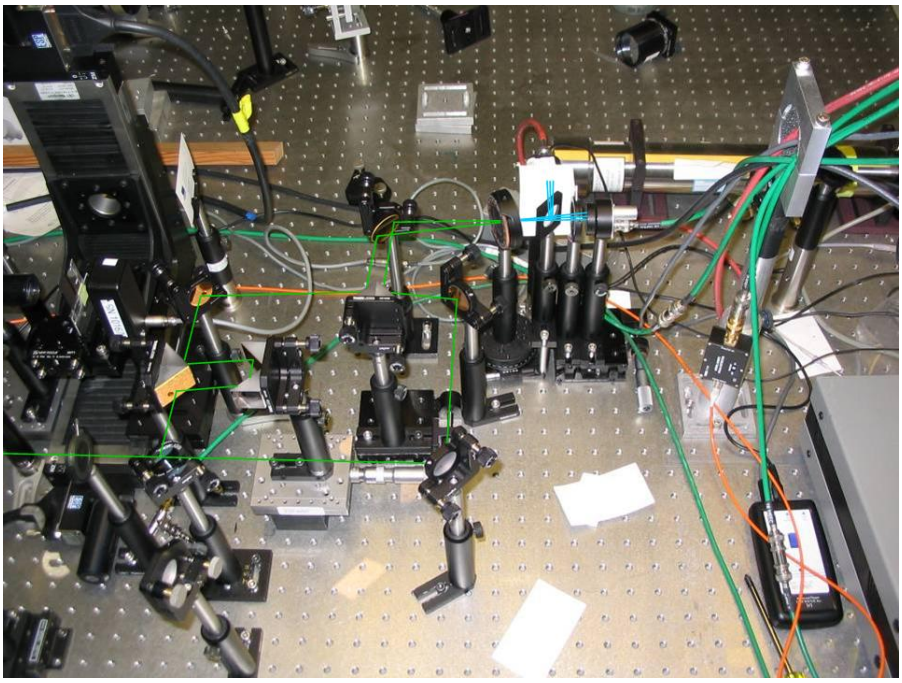

Figure 4. Photo of the autocorrelator setup. The infrared pulses are shown in green, while doubled light is shown in blue.

a pellicle beamsplitter, and one arm had an adjustable delay. After passing through their respective paths, the beams were directed parallel to one another and then into an off-axis parabolic mirror. This focused and crossed the beams at the same position on a nonlinear barium borate (BBO) crystal, which was mounted on a rotation stage to adjust the angle of its optic axis. At the proper angle, pulses of double the frequency (shown in blue in Fig. 3) were produced between the two crossed beams, as long as the pulses were coincident on the crystal. A beam sampler was used to direct some of the doubled light onto a CCD to optimize the alignment. The remainder was captured by a photodiode, whose signal was integrated in a Stanford Research Systems SR250 gated integrator, and then passed to the data acquisition system (DAQ) for recording. We obtained an autocorrelation trace by varying the delay in one arm of the interferometer, and thus the temporal overlap of the beams on the crystal, and observing the resulting signal on the diode. A picture of the autocorrelator is shown in Fig. 4.

Our data acquisition system consisted of a Dell Precision 330 computer with a 1.8 GHz Pentium 4 processor and 1 GB RAM. It contained a Newport ESP6000 motion controller card and a National Instruments PCI-MIO-16E-4 data acquisition board. The motion controller was used to move, and read back position data from, the translation stages on which the sample was mounted. The DAQ board was used to acquire analog voltage data from the pyroelectric detectors and photodiodes, as well as control a motorized flipper used as a beam stop to begin and end sets of damage data. LabVIEW software was used to automate the data taking and perform initial processing of the data. Our pyroelectric detectors output signals on the time scale of 100 µs, slow enough so that an entire trace could be captured by the 100 kHz ADCs in the DAQ board. The signal level was taken to be the maximum value of the pyro voltage during the trace.

For each wavelength tested, we first measured the spectral content of the pulses to confirm the absence of shorter wavelength light. Such light could have come from the Ti:sapphire pump at 800 nm, the signal wavelength when the idler was desired, or in the visible range from the pump mixed with the signal or the idler within the OPA. The beam was coupled via fiber to an optical spectrum analyzer (OSA). We first acquired a spectrum over the entire 600–1700 nm range of the OSA; a sample spectrum from a 1550 nm run is shown in Fig. 5. The noise floor in the spectrum shown is determined by the sensitivity of the OSA. For higher sensitivity, we also acquired spectra over smaller ranges centered on wavelengths where shorter-wavelength contamination might have been present. Since we expect that such contamination would have been narrow-band, centered only at the wavelengths of light produced within the OPA, this was sufficient to confirm the absence of additional wavelengths in the pulses. In each case we verified that the level of any shorter wavelength light was

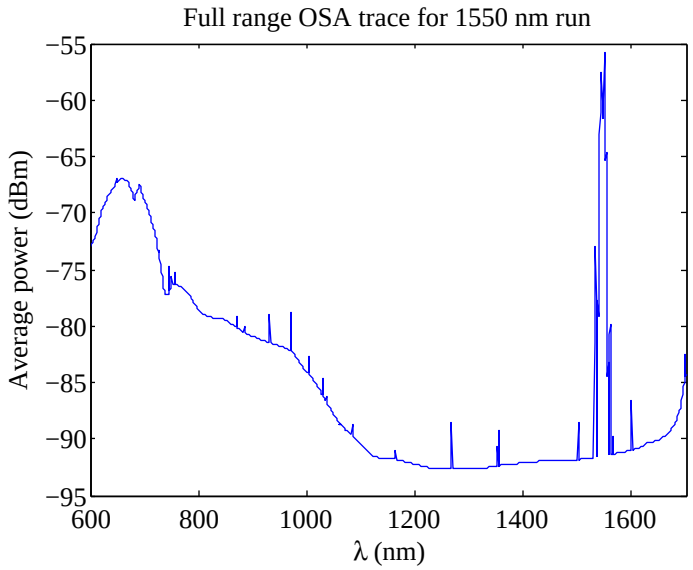

Figure 5. An OSA trace for the 1550 nm run covering the full range of the spectrum analyzer.

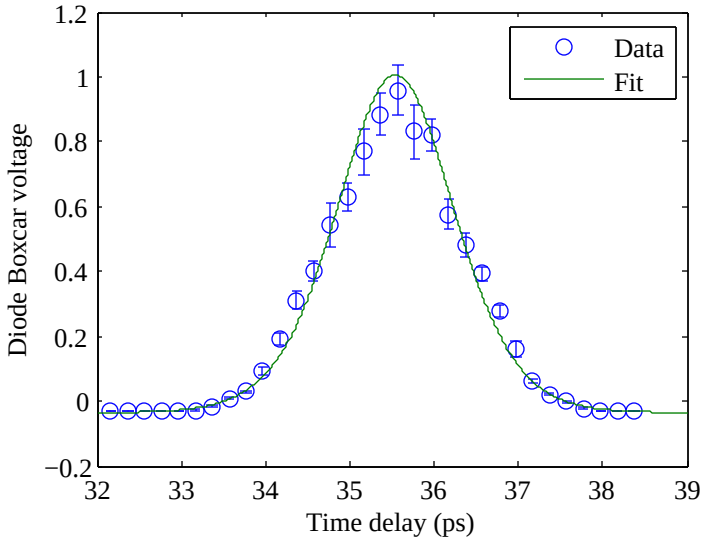

Figure 6. The autocorrelation trace for the 1550 nm run.

at least 30 dB less than the wavelength of interest.

Next, we took an autocorrelation trace to measure the pulse duration. We adjusted the delay arm of the autocorrelator in a pseudorandom sequence in order to prevent slow pulse energy drifts from causing a systematic error. While the delay stage was manual, the DAQ prompted the user to set each delay at the proper micrometer reading in order to form the pseudorandom sequence. For each delay, we acquired diode levels for 1000 shots. We then fit the data to an autocorrelation profile, assuming a sech^2 temporal profile of the incident pulse, as is the case for passively modelocked lasers.[10] The autocorrelation trace for the 1550 nm run, along with the fit, is shown in Fig. 6. From the fit we deduce a FWHM pulse duration of 1.06 ± 0.01 ps.

After the autocorrelation trace was taken, the final focus lens was adjusted to place the beam waist just in front of the sample surface. This was to ensure that maximum fluence occurred on the sample surface rather than in the bulk, so that the transverse spot-size measurements would yield relevant results. Also, the HeNe beam was spatially overlapped with

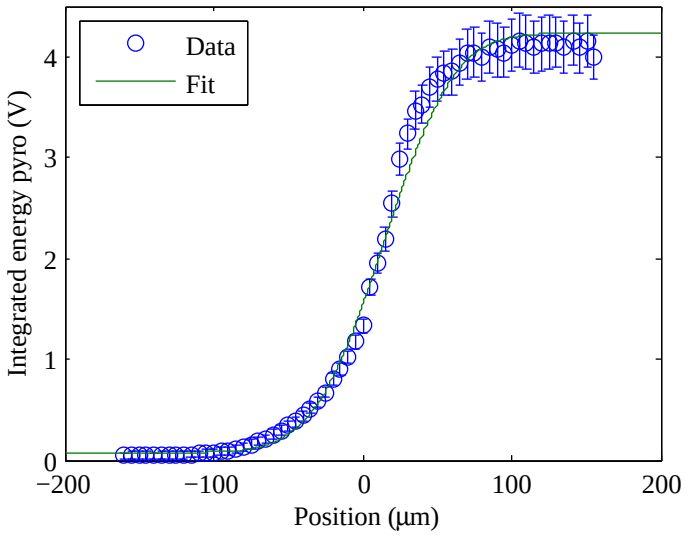

Figure 7. The horizontal knife edge measurement for the 1550 nm run.

the infrared pulses and one damage spot was created to confirm that the pulse energy was sufficient and the focus was tight enough for damage to occur. Once this was complete, the transverse spot sizes were measured using the knife-edge technique. This was accomplished using razor blades glued to the same microscope slide as the silicon sample so that their edges were in the same plane as the sample surface. The platform holding the sample and the razor blades was mounted on a pair of Newport M-UTM150CC1DD motorized linear stages to allow for motion in both directions in the plane of the sample. A Molectron P1-45 pyroelectric detector was placed behind the knife edges to capture any unblocked light. A LabVIEW VI was used to automatically move the stages, in one dimension at a time, to adjust the position of a knife edge in pseudorandom order. At each position, we acquired pyro signal levels for 1000 shots. The horizontal knife edge measurement for the 1550 nm run is shown in Fig. 7. We fit the data to an error function, which is the curve that results from integrating a Gaussian spot intensity profile. For this knife-edge scan, we acquire a spot width of $w_x = 74.3 \pm 2.2\,\mu\text{m}$.

As a final setup step, we calibrated the sensitive pyroelectric detector used to measure pulse energy, also a Molectron P1-45. This was necessary for each wavelength because the reflectivity of the pellicle beam sampler varied with wavelength. We calibrated the Molectron detector against an Ophir Optronics PE10 energy detector; since the Ophir detector had an absolute calibration in our wavelength range, this allowed us to have an absolute calibration of the Molectron detector at each wavelength. We placed the Ophir detector behind the sample and used the stages to remove the sample from the beam path. This ensured that the Ophir detector was reading the pulse energies after the beam passed through its transport through the sample and therefore was measuring the actual incident pulse energies. We acquired approximately 1200 shots on both the Ophir detector and the Molectron sensor for a range of energies. A linear fit was then performed to obtain the calibration.

3. DATA ANALYSIS AND RESULTS

Once the setup was complete for a particular wavelength, damage data were taken. For each event, the pulses were allowed to illuminate the sample by removing a beam stop, and infrared pulse energy and reflected HeNe power were then acquired on a shot-to-shot basis. Since the data acquisition rate was limited to ≈ 100 Hz, less than the repetition rate of the laser, not all samples were acquired. The acquisition was stopped, and the beam stop reinserted, when either the HeNe power decreased, indicating damage, or a certain amount of time, usually ≥ 100 s, had elapsed with no damage. Each set of pulse energy and HeNe power data, taken between the time the beam stop was initially removed and the time the acquisition was stopped, constituted one "event." Events were taken both above and below the damage threshold, and the sample was moved at least 1 mm between each event to avoid geometric deformities from one damage spot affecting subsequent measurements.

A sample event is plotted in Fig. 8. We notice that the reflected HeNe power increases for a fraction of a second before

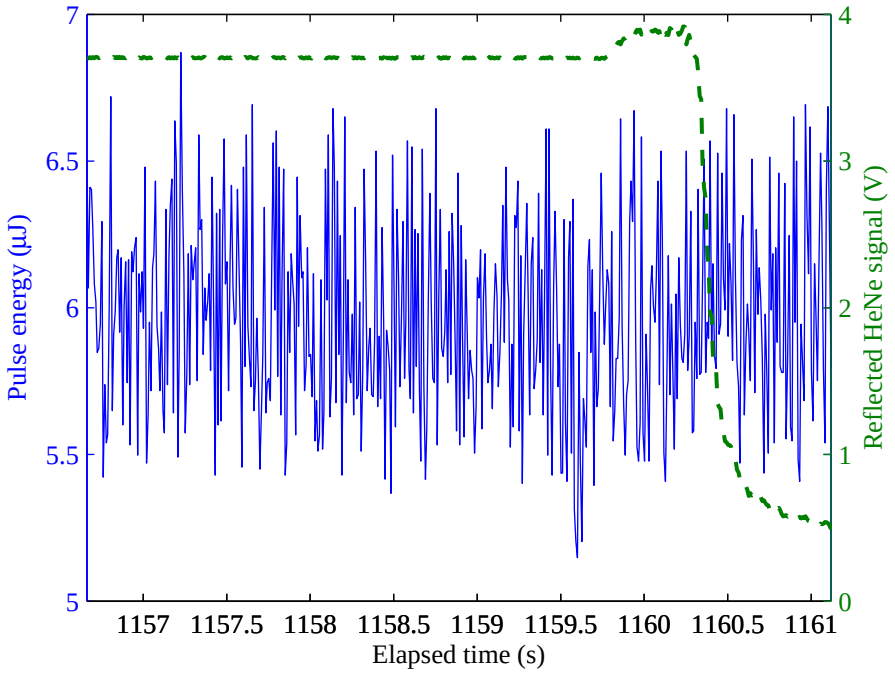

Figure 8. A sample event. Shown here are data from the last several seconds of an event in which damage occurred after about 1160 s. The solid line shows a trace of the acquired pulse energy, and the dashed line shows the reflected HeNe power.

falling off. This is ostensibly due to additional focusing from the silicon surface as the damage morphology develops. Indeed, we observed using a CCD image of the reflected HeNe light that the mode pattern changes for about a second during damage before finally disappearing.

From the multiple-shot data in this event and others like it, it is not immediately clear how to compute the measured damage threshold. We assume that damage was initiated by a single pulse, with further damage occurring in each subsequent shot due to the field enhancement resulting from the initial deformation of the surface. That pulse may or may not have been acquired, and the data do not tell us how long before the visible onset of damage the pulse occurred. However, we can make a maximum likelihood estimate for the damage threshold based on a few assumptions. First, the damage process is deterministic, as reported in Ref. 7, so damage did occur after a pulse that exceeded the threshold and did not otherwise. Second, at least one pulse with energy above threshold therefore must have occurred within the 1000 acquired shots before the visible onset of damage. Third, no such shot occurred more than 1000 shots before the visible onset of damage, or more than 1000 shots before the end of an event in which no damage was observed.

Using these assumptions, we form a maximum likelihood estimate of the damage threshold as follows. The data for each event include a sequence of N acquired pulse energies, $\{U_i\}_{i=1}^{N}$, as well as a sequence of reflected HeNe diode voltages acquired simultaneously. If damage occurred during the event, we define the "damage index" i_d to be the index of the first shot in which the reflected HeNe diode read more than 0.5 V below the initial reading at the start of the event. We then divide the event into "blocks" of 1000 acquired events as follows: If damage occurred, we have assumed that the shot that initiated it occurred within the 1000 acquired shots before i_d. The index of the last shot where we know damage did not occur is therefore $i_1 = \max(i_d - 1000, 0)$. If $i_1 = 0$, then there is no shot we can be sure did not cause damage. We call the set of pulse energies $\{U_i\}_{i=i_1+1}^{i_d}$ the "damage block." We then divide the acquired pulse energies which we know did not cause damage into "no-damage blocks" of 1000 pulses each, starting with the first acquired pulse. If no damage occurred during the event, we let $i_1 = N$; then regardless of whether damage occurred there are $\lfloor i_1/1000 \rfloor$ no-damage blocks in the event.

Because we did not acquire the energy of each incident pulse, we do not use the acquired pulse energies directly to form our damage threshold estimate. Rather, we use the acquired pulse energies to form a statistical description of each

block, and use those statistical parameters to estimate the threshold. To obtain the number of incident pulses in a block, we need to know the ratio r of incident to acquired pulses. The DAQ records the total elapsed time T for the event; then for the known laser repetition rate f_{rep} we have $r = f_{\text{rep}}T/N$. For each block B, we fit the pulse energies in that block to an asymmetric Gaussian distribution, with peak μ and RMS widths σ_1 and σ_2 for $U < \mu$ and $U > \mu$ respectively. We ignore the pulse energies with $U < \mu$, and consider the distribution of pulse energies in a block to be a one-sided Gaussian with peak $\mu_B = \mu$ and RMS width $\sigma_B = \sigma_2$. We can justify this because if damage occurred, it is unlikely that it was a pulse with such low energy that caused it, when pulses with higher energies were present. Conversely, if damage did not occur, the fact that a relatively low-energy pulse did not cause damage yields little information. The probability density function for pulse energy U within block B is therefore

$$f(U) = \begin{cases} \sqrt{\frac{2}{\pi}} \frac{1}{\sigma_B} e^{-(U-\mu_B)^2/2\sigma_B^2} & U \geq \mu_B, \\ 0 & \text{otherwise.} \end{cases} \tag{1}$$

We estimate the number of relevant incident pulses within the block to be $N_B = r|\{U \in B \mid U \geq \mu_B\}|$.

We can now form a likelihood function from these statistical parameters. For a given block B, let $P_1(U_{\text{th}})$ be the probability that a single incident pulse from block B does not cause damage if the pulse energy damage threshold is U_{th}. This is the probability that a pulse energy $U < U_{\text{th}}$. From Eq. (1) we have that $P_1(U_{\text{th}}) = 0$ if $U_{\text{th}} \leq \mu_B$, and that for $U_{\text{th}} \geq \mu_B$,

$$\begin{aligned} P_1(U_{\text{th}}) &= \int_{\mu_B}^{U_{\text{th}}} \sqrt{\frac{2}{\pi}} \frac{1}{\sigma_B} e^{-(U-\mu_B)^2/2\sigma_B^2} \, dU \\ &= \operatorname{erf}\left(\frac{U_{\text{th}} - \mu_B}{\sqrt{2}\sigma_B} \right). \end{aligned}$$

Then the probability $P_B(U_{\text{th}})$ that no damage occurs within the block is the probability that none of the incident pulses initiate damage, or

$$P_B(U_{\text{th}}) = P_1(U_{\text{th}})^{N_B} = \begin{cases} \left[\operatorname{erf}\left(\frac{U_{\text{th}} - \mu_B}{\sqrt{2}\sigma_B} \right) \right]^{N_B} & U_{\text{th}} \geq \mu_B, \\ 0 & \text{otherwise.} \end{cases}$$

This equation makes physical sense, since not only is damage more likely to occur if the mean pulse energy is increased, it is also more likely to occur if the pulse energy jitter increases. Increased jitter makes it more likely that there will be a pulse above damage threshold, underscoring the importance of stable laser sources for high-power photonic applications.

To compute the likelihood function we use all the blocks acquired during the course of a run at the given wavelength. Let $\mathcal{B}_d$ be the collection of damage blocks for the run, and let $\mathcal{B}_{nd}$ be the collection of no-damage blocks. Our likelihood function is then

$$L(U_{\text{th}}) = \prod_{B \in \mathcal{B}_{nd}} P_B(U_{\text{th}}) \cdot \prod_{B \in \mathcal{B}_d} \left[1 - P_B(U_{\text{th}}) \right].$$

To find the value of U_{th} with maximum likelihood, we compute the negative log likelihood, given by the function

$$\chi^2(U_{\text{th}}) = -\sum_{B \in \mathcal{B}_{nd}} \log P_B(U_{\text{th}}) - \sum_{B \in \mathcal{B}_d} \log \left[1 - P_B(U_{\text{th}}) \right].$$

We compute the χ^2 function numerically, and use the MATLAB minimization routine `fminbnd` to find the value of U_{th} which minimizes χ^2 as well as the minimum value χ_0^2. We then use the routine `fzero` to find the pulse energies U_+ and U_- above and below U_{th}, respectively, for which $\chi^2(U_+) = \chi^2(U_-) = \chi_0^2 + 1$, and defined the error on U_{th} to be $(U_+ - U_-)/2$. For instance, for the run at $\lambda = 1550\,\text{nm}$, the threshold was $(7.78 \pm 0.05)\,\mu\text{J}$.

We now have the information required to reconstruct the damage threshold fluence the material; it is given by $F_{\text{th}} = 2U_{\text{th}}/\pi w_x w_y$. We obtained data sets for $\lambda = 1550\,\text{nm}$, 1700 nm, 1900 nm, 2100 nm, and 2256 nm. The damage threshold results are plotted in Fig. 9. The data point at 2100 nm was repeated several months after the initial point was taken, in order to check the consistency of the setup; we found the two points to be within reasonable statistical error of one another. Comparison among damage thresholds at different wavelengths is complicated by the fact that each measurement was taken

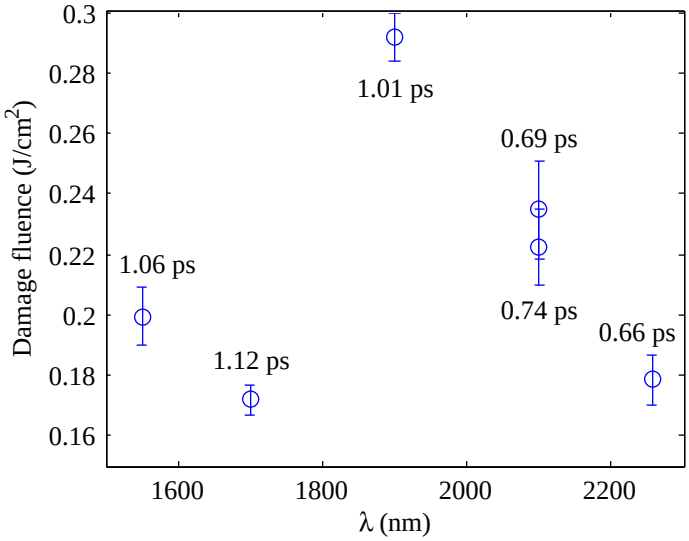

Figure 9. Damage thresholds for a range of wavelengths. The measured FWHM pulse width at each wavelength is shown next to the corresponding point.

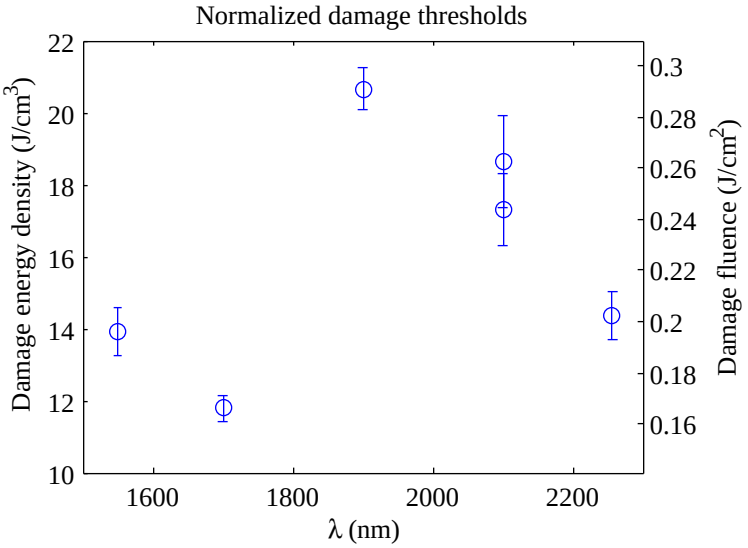

Figure 10. Damage thresholds, normalized for pulses with 1 ps FWHM duration. Scales are shown for both fluence and energy density; with the normalization to a fixed pulse duration they are proportional to one another.

using a different pulse duration. We can attempt to remove the pulse duration dependence using the empirical scaling law of $F_{\text{th}} \sim \tau^{0.3}$ reported in Ref. 11. However, we should note that the result in Ref. 11 was determined for oxide thin films and might not be applicable to silicon. The damage fluence, normalized for pulses with 1 ps FWHM duration, are plotted in Fig. 10.

4. DISCUSSION

We first notice that the damage threshold of silicon at these wavelengths is low compared to larger-bandgap materials that have been previously measured. The normalized fluence thresholds of 160–300 mJ/cm^2 are an order of magnitude lower than those for fused silica, CaF_2, and other fluorides.[12] It is also several times lower than the thresholds for the larger-

bandgap semiconductors ZnS and ZnSe reported in Ref. 13 for wavelengths of 400 and 800 nm and in the mid-infrared. In addition, the thresholds are quite similar to those at 800 nm, where silicon is opaque.[6]

We also notice that the damage threshold does indeed increase as the wavelength approaches the two-photon absorption threshold, between 1700 nm to 1900 nm. This is reasonable, since we would not expect a sharp cutoff from an MPI-dominated process because silicon has an indirect bandgap. At wavelengths longer than 1900 nm, we then see a decrease in damage fluence. This may be due to the same mechanism as reported in Ref. 13, in which the damage threshold decreased at longer wavelengths because of the increased probability of tunnel ionization. Therefore, the increase in damage threshold from 1700 nm to 1900 nm is not dramatic enough to indicate that the damage process is highly dominated by the MPI effect. In addition, since the increase in threshold would only increase the sustainable electric field by $\sim 30\%$, the decision whether to use longer wavelengths outside the telecom band in a photonics application might be guided by other considerations. And because of the low breakdown threshold relative to other dielectrics, the choice of material for high-power devices remains an open question.

ACKNOWLEDGMENTS

The author would like to thank R. Siemann, I. Blumenfeld, C. Clayton and M. Tang for helpful advice and R. Ischebeck and J. Spencer for the silicon sample, and extend special thanks to D. Simanovskii, G. Marcus, K. Cohn and D. Palanker of the Hansen Experimental Physics Laboratory at Stanford University for use of the laser system and assistance with the OPA. Work supported by Department of Energy contracts DE-AC02-76SF00515 (SLAC) and DE-FG03-97ER41043-II (LEAP).

REFERENCES

1. D. F. Edwards, "Silicon," in *Handbook of Optical Constants*, E. D. Palik, ed., **1**, p. 547, Academic Press, 1985.
2. IMRA America, Inc., `http://www.imra.com/`.
3. K. M. Ho, C. T. Chan, C. M. Soukoulis, R. Biswas, and M. Sigalas, "Photonic band gaps in three dimensions: new layer-by-layer periodic structures," *Solid State Commun.* **89**, pp. 413–416, Feb 1994.
4. E. Colby, G. Lum, T. Plettner, and J. Spencer, "Gamma radiation studies on optical materials," *IEEE Trans. Nucl. Sci.* **49**, pp. 2857–2867, Dec 2002.
5. B. Cowan, "Three-dimensional photonic crystal laser-driven accelerator structures," in *Twelfth Advanced Accelerator Concepts, Lake Geneva, WI, 2006*, M. Conde and C. Eyberger, eds., pp. 844–850, American Institute of Physics, (Melville, NY), 2006.
6. P. Allenspacher, B. Hüttner, and W. Riede, "Ultrashort pulse damage of Si and Ge semiconductors," in *Laser-Induced Damage in Optical Materials: 2002 and 7th International Workshop on Laser Beam and Optics Characterization*, G. J. Exarhos, A. H. Guenther, N. Kaiser, K. L. Lewis, M. J. Soileau, C. J. Stolz, A. Giesen, and H. Weber, eds., *Proceedings of SPIE* **4932**, pp. 358–365, SPIE, (Bellingham, WA), 2003.
7. A. P. Joglekar, H. Liu, G. J. Spooner, E. Meyhöfer, G. Mourou, and A. J. Hunt, "A study of the deterministic character of optical damage by femtosecond laser pulses and applications to nanomachining," *Appl. Phys. B* **77**, p. 25, Aug 2003.
8. M. Lenzner, J. Kruger, S. Sartania, Z. Cheng, C. Spielmann, G. Mourou, W. Kautek, and F. Krausz, "Femtosecond optical breakdown in dielectrics," *Phys. Rev. Lett.* **80**, pp. 4076–4079, May 1998.
9. L. V. Keldysh, "Ionization in the field of a strong electromagnetic wave," *Sov. Phys. JETP* **20**, pp. 1307–1314, May 1965.
10. A. E. Siegman, *Lasers*, University Science Books, Mill Valley, CA, 1986.
11. M. Mero, J. Liu, W. Rudolph, D. Ristau, and K. Starke, "Scaling laws of femtosecond laser pulse induced breakdown in oxide films," *Phys. Rev. B* **71**, p. 115109, 2005.
12. B. C. Stuart, M. D. Feit, S. Herman, A. M. Rubenchik, B. W. Shore, and M. D. Perry, "Nanosecond-to-femtosecond laser-induced breakdown in dielectrics," *Phys. Rev. B* **53**, pp. 1749–1761, Jan 1996.
13. D. M. Simanovskii, H. A. Schwettman, H. Lee, and A. J. Welch, "Midinfrared optical breakdown in transparent dielectrics," *Phys. Rev. Lett.* **91**, p. 107601, Sep 2003.